

Collider Tests of (Composite) Diphoton Resonances

Emiliano Molinaro, Francesco Sannino, and Natascia Vignaroli

CP³-Origins and the Danish IAS, University of Southern Denmark, Campusvej 55, DK-5230 Odense M, Denmark

We analyze the Large Hadron Collider sensitivity to new pseudoscalar resonances decaying into diphoton with masses up to scales of few TeVs. We focus on minimal scenarios where the production mechanisms involve either photon or top-mediated gluon fusion, partially motivated by the tantalizing excess around 750 GeV reported by ATLAS and CMS. The two scenarios lead respectively to a narrow and a wide resonance. We first provide a model-independent analysis via effective operators and then introduce minimal models of composite dynamics where the diphoton channel is characterized by their topological sector. The relevant state here is the pseudoscalar associated with the axial anomaly of the new composite dynamics. If the Standard Model top mass is generated via four-fermion operators the coupling of this state to the top remarkably explains the wide-width resonance reported by ATLAS. Beyond the excess, our analysis paves the way to test dynamical electroweak symmetry breaking via topological sectors.

I. THE RELEVANCE OF THE DIPHOTON CHANNEL

The diphoton channel has proved extremely successful in discovering new (pseudo)scalar particles such as the Higgs boson [1, 2]. Earlier π_0 and η' decays into $\gamma\gamma$ provided instrumental to demonstrate the composite nature of the QCD hadrons. Furthermore, a tantalizing excess around 750 GeV has been reported by the LHC experimental collaborations [3, 4] in the current run at $\sqrt{s} = 13$ TeV. More specifically, with 3.2 fb^{-1} , ATLAS observes an excess in the number of events, respectively of about 7.8 and 4.3, for the diphoton invariant mass bins at 730 and 770 GeV. This corresponds to a local significance of 3.9σ at 750 GeV, under the assumption of a large width of about 45 GeV. With 2.6 fb^{-1} CMS measures an excess around 760 GeV, corresponding to a local significance of 2.6σ .

It is therefore timely to investigate the LHC reach and constraints from the diphoton channel. Because of the intriguing excess around 750 GeV, we first specialize our analysis around this energy range. Minimal models that can explain the excess entail gluon fusion production through new colored states [5–10] or photon fusion production [11–14] that typically lead to a narrow resonance (see also [15, 16]). If a wide-width scenario, currently favored by ATLAS [3], is confirmed, it can be achieved via a direct coupling to the top quark [17, 18]. This induces the production of the pseudoscalar resonance via top-mediated gluon fusion. Alternative ways to obtain a wide width are via exotic decay topologies [19–24] or invoking a coupling to an invisible sector [25–27].

Here we therefore consider two production mechanisms, the photon and top-mediated gluon fusion. We will first rely on an effective field theory approach and then consider minimal models of composite dynamics. We discuss the current constraints and excesses coming from the LHC run at $\sqrt{s} = 8$ TeV (LHC-8) as well as the run at $\sqrt{s} = 13$ TeV (LHC-13). We observe that when the resonance is photo-produced one can constrain it up to high mass values of the order of 5 TeV with around 100 fb^{-1} . If the diphoton resonance is produced via top-mediated gluon fusion the reach is up to 2 TeV with 100 fb^{-1} , due to the quick drop of the production cross section with its mass.

Minimal models of composite dynamics all predict a pseudoscalar state with specific couplings to the electroweak (EW) gauge bosons which arise from the topological sector of the underlying theory [5, 28]. This state is the analogue of the η' of QCD. This makes the models ideal case-studies for the diphoton channel. The composite pseudoscalar resonance also offers a natural explanation for the observed excess at 750 GeV, as shown in [5]. Other composite realizations have been explored in [18, 29–36].

We first review the effective Lagrangian for minimal models of composite dynamics augmented by the gauged version of the Wess-Zumino-Witten term [37–42]. We then move to its phenomenology in the two limits of photon and gluon fusion production of the η' -like state. We will see that if the Standard Model (SM) top mass is generated via four-fermion operators, the coupling of this state to the top naturally explains the wide-width resonance reported by ATLAS.

Our results demonstrate that topological sectors stemming directly from the underlying dynamics give rise to novel signatures in the diphoton and EW channels that open a new avenue to test natural theories of EW symmetry breaking at present and near future collider experiments. In that respect, our analysis complements phenomenological studies of composite dynamics that, so far, have been mostly focused on spin-one resonances [43, 44].

The paper is structured as follows: in section II we set up the analysis via an effective operator framework and study the photon and the top-mediated gluon fusion production mechanisms. We also compare with current collider limits and discuss the observed excesses at 750 GeV. We then determine the LHC-13 reach for higher masses. In section III we introduce the minimal models of composite dynamics and their effective Lagrangian including the topological terms. For the two envisioned production mechanisms we analyze the LHC-13 reach and constraints stemming from these terms. We finally offer our conclusions in section IV. Further details related to the topological terms can be found in the appendix.

II. LHC-13 REACH ON DIPHOTON RESONANCES

We derive the LHC-13 reach on diphoton resonances via an effective approach in the two hypotheses of dominant photon and gluon fusion production mechanisms. Clearly the final result depends sensitively on how the new physics couples to SM degrees of freedom. We encode the new physics in the effective theory below:

$$\begin{aligned} \mathcal{L}_{\text{eff}} = & -iy_t \frac{m_t}{v} a \bar{t}\gamma_5 t - \frac{c_{GG}}{8v} a \text{Tr} \left[G^{\mu\nu} \tilde{G}_{\mu\nu} \right] \\ & - \frac{c_{AA}}{8v} a A^{\mu\nu} \tilde{A}_{\mu\nu} - \frac{c_{AZ}}{4v} a A^{\mu\nu} \tilde{Z}_{\mu\nu} - \frac{c_{WW}}{4v} a W^{+\mu\nu} \tilde{W}_{\mu\nu}^- - \frac{c_{ZZ}}{8v} a Z^{\mu\nu} \tilde{Z}_{\mu\nu} \end{aligned} \quad (1)$$

in which a is a new pseudoscalar boson of mass m_a in the TeV energy range, $v = 246$ GeV is the EW scale, and $\tilde{V}^{\mu\nu} = \epsilon^{\mu\nu\rho\sigma} V_{\rho\sigma}$. Note that we have reabsorbed the scale of new physics Λ_{NP} into the definition of the effective

couplings

$$c_{VV} \approx \frac{1}{4\pi} \frac{v}{\Lambda_{\text{NP}}}, \quad (2)$$

whose specific value depends on the underlying theory. We neglect in \mathcal{L}_{eff} the direct couplings of a to the SM fermions except for the top quark t .

As the c_{VV} related operators are non-renormalizable, they arise via either non-perturbative dynamics or loop corrections. This implies that these coefficients contain both information about new physics and also the calculable SM contributions coming from the renormalizable interactions of a with SM particles, in this case the top quark. Hence, \mathcal{L}_{eff} can be viewed as a conservative but sufficiently general effective description of a new pseudoscalar state. In this simple picture, we will not invoke the presence of new colored vector-like states that can also serve to produce this state [5–10]. This means that, in our case, the effective coupling to the gluons c_{GG} is entirely given by the top loop and reads

$$c_{GG} = y_t \frac{\alpha_S}{2\pi} F\left(\frac{m_a^2}{4m_t^2}\right), \quad (3)$$

where m_t is the top mass, α_S is the strong coupling constant and $F(x) = -\frac{1}{4x} \left(\ln \frac{\sqrt{x} + \sqrt{x-1}}{\sqrt{x} - \sqrt{x-1}} - i\pi \right)^2$ for $x > 1$ [45]. As for the other c_{VV} , the top loop contribution is included but we will keep them free to accommodate the effects of new non-colored states. In our analysis we will consider two limits, one in which the coupling to the top is order $y_t \simeq 1$, still within the perturbative regime, and the one in which $y_t = 0$. In the first case we will have a top mediated gluon fusion production of the new state a , while in the second we will have the photon production. In the case $y_t \neq 0$ the presence of the top, as we shall demonstrate, naturally enhances the total width of a up to $\Gamma_{\text{tot}}(a)/m_a \approx 0.06$.

From (1) the effective partial decay rates read:

$$\Gamma(a \rightarrow gg) = \frac{m_a^3}{8\pi} \frac{|c_{GG}|^2}{v^2} \quad (4)$$

$$\Gamma(a \rightarrow \gamma\gamma) = \frac{m_a^3}{64\pi} \frac{c_{AA}^2}{v^2}, \quad (5)$$

$$\Gamma(a \rightarrow \gamma Z) = \frac{m_a^3}{32\pi} \frac{c_{AZ}^2}{v^2} \left(1 - \frac{m_Z^2}{m_a^2}\right)^3, \quad (6)$$

$$\Gamma(a \rightarrow ZZ) = \frac{m_a^3}{64\pi} \frac{c_{ZZ}^2}{v^2} \left(1 - \frac{4m_Z^2}{m_a^2}\right)^{3/2}, \quad (7)$$

$$\Gamma(a \rightarrow W^+W^-) = \frac{m_a^3}{32\pi} \frac{c_{WW}^2}{v^2} \left(1 - \frac{4m_W^2}{m_a^2}\right)^{3/2}, \quad (8)$$

$$\Gamma(a \rightarrow t\bar{t}) = y_t^2 \frac{3m_a}{8\pi} \frac{m_t^2}{v^2} \sqrt{1 - \frac{4m_t^2}{m_a^2}} \quad (9)$$

As a logical step we start by plotting the production cross sections for various mechanisms relevant at LHC-13 as function of m_a stemming from our effective action. These are summarized in Fig. 1. For illustration, in the plot we assume $y_t = 1$ for the gluon fusion production and $c_{VV} = 1$ for the other processes.

The photon fusion production mechanism receives three contributions: the leading one (ranging from 60% to 85% for m_a from 0.5 to 5 TeV) comes from incoherent/inelastic scattering, whereas two subdominant contributions arise from the semi-coherent and the coherent scattering processes [46, 47], where either one of or both the colliding protons remain intact. We determine the production cross section at leading-order (LO) with MadGraph5 [48], by using the NNPDF2.3QED [49] set of parton distribution functions (PDFs). The improved Weizsaecker-Williams formula [50] is automatically employed by MadGraph5 to simulate low virtuality photon emission by proton beams [48]. This allows to estimate the elastic and semi-elastic contributions ¹. The largest error on the cross section comes from the uncertainty on the photon PDF. In particular, for the NNPDF2.3QED set used in our analysis the quoted uncertainty is typically of the order of 50% [49], but it might be even bigger in the large x region, $x \gtrsim 0.1$ ($m_a \gtrsim 1.3$ TeV at LHC-13), due to the lack of experimental data. Our estimates are thus subject to $\mathcal{O}(1)$ corrections at large m_a

¹ Our production cross section at $m_a = 750$ GeV agrees with the results in [11, 13].

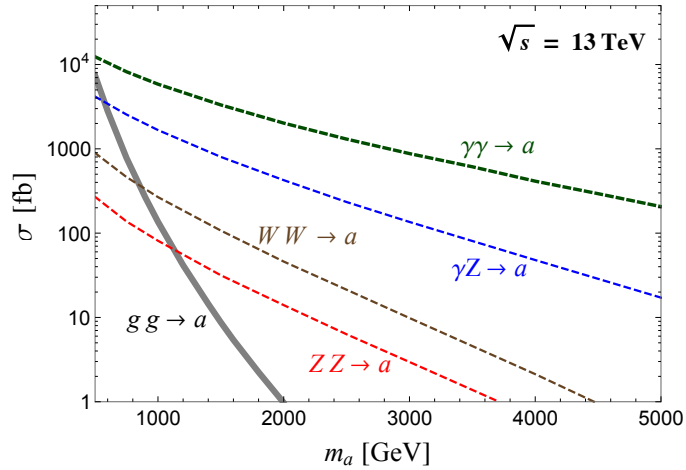


FIG. 1. The production cross section of the pseudoscalar resonance at LHC-13 as function of its mass for the different modes: $\gamma\gamma$, γZ , WW and ZZ fusion (with $c_{AA} = c_{AZ} = c_{WW} = c_{ZZ} = 1$) and top-mediated gluon fusion (with $y_t = 1$), see (1). The gluon fusion cross section has been evaluated at NLO in QCD. The photon fusion includes the dominant incoherent as well as the subdominant semi-coherent and coherent contributions.

[14, 49]². Both the coherent and incoherent photon emission are taken into account in the γZ production cross section. The latter and the remaining vector boson fusion contributions from ZZ and WW channels are also computed with MadGraph5 and are subdominant when the effective couplings c_{VV} arise from a common source of new physics.

The gluon fusion cross section occurring for a non vanishing y_t includes K-factor corrections up to the next-to-leading order (NLO) in QCD, which have been evaluated by using the model in [52], with MadGraph5_aMC@NLO [53]. We deduce K-factors ranging from 2.1 to 1.8 for $0.5 \text{ TeV} \lesssim m_a \lesssim 2 \text{ TeV}$. Interestingly, we observe the general feature that the production cross section stemming from the top-mediated gluon fusion drops quickly with m_a . This is due to the combined effect of the scaling of the gluon PDF at large x and the top-loop function, that vanishes in the limit $m_a/m_t \rightarrow \infty$. Another minor effect comes from the running of the strong coupling α_S .

On the contrary, the production cross sections associated with the weak gauge bosons, and especially the photon, have a much gentler scaling with m_a . This means that the reach with respect to the new pseudoscalar mass m_a is much wider when the new state is produced via the weak gauge boson rather than via the top-mediated gluon fusion.

A. Production via photon fusion

We will focus now on a very minimal scenario where a does not couple directly to the top, that means setting $y_t = 0$ in (1). Here the production relies on purely EW channels, with the dominant contribution coming from photon fusion, as evident from Fig. 1. The signal cross section at LO in the narrow-width approximation can be expressed as

$$\sigma(pp \rightarrow a \rightarrow \gamma\gamma) = \frac{8\pi^2 \Gamma(a \rightarrow \gamma\gamma)}{m_a} \frac{d\mathcal{L}^{\gamma\gamma}}{dm_a^2} \text{BR}(a \rightarrow \gamma\gamma), \quad (10)$$

where $d\mathcal{L}^{\gamma\gamma}/dm_a^2$ denotes the photon luminosity function, which can be extracted from Fig. 1. From (5) and (10) it is clear that the a production cross section $\sigma(pp \rightarrow a)$ depends quadratically on c_{AA} . In our study of the reach/constraints on diphoton resonances produced by photon fusion we consider a fixed value for $\text{BR}(a \rightarrow \gamma\gamma)$, that is $\text{BR}(a \rightarrow \gamma\gamma)=0.6$. This choice is motivated by the specific composite dynamics explanation of the 750 GeV diphoton excess, which will be discussed in section III. Nevertheless, our results do not depend on this specific choice, since a difference in $\text{BR}(a \rightarrow \gamma\gamma)$ will only imply a rescaling of the effective coupling c_{AA} . This results in an overall vertical shift of the constraints in the plane (m_a, c_{AA}) .

We start by examining the region of the effective coupling space able to reproduce the diphoton excess at $m_a \simeq 750 \text{ GeV}$. This is shown in the left plot in Fig. 2, where the green area in the (m_a, c_{AA}) plane is the region of the

² For example, by using the other available MRST2004QED PDF set [51] we obtain a cross section smaller by a factor of ~ 1.7 for $m_a = 2 \text{ TeV}$.

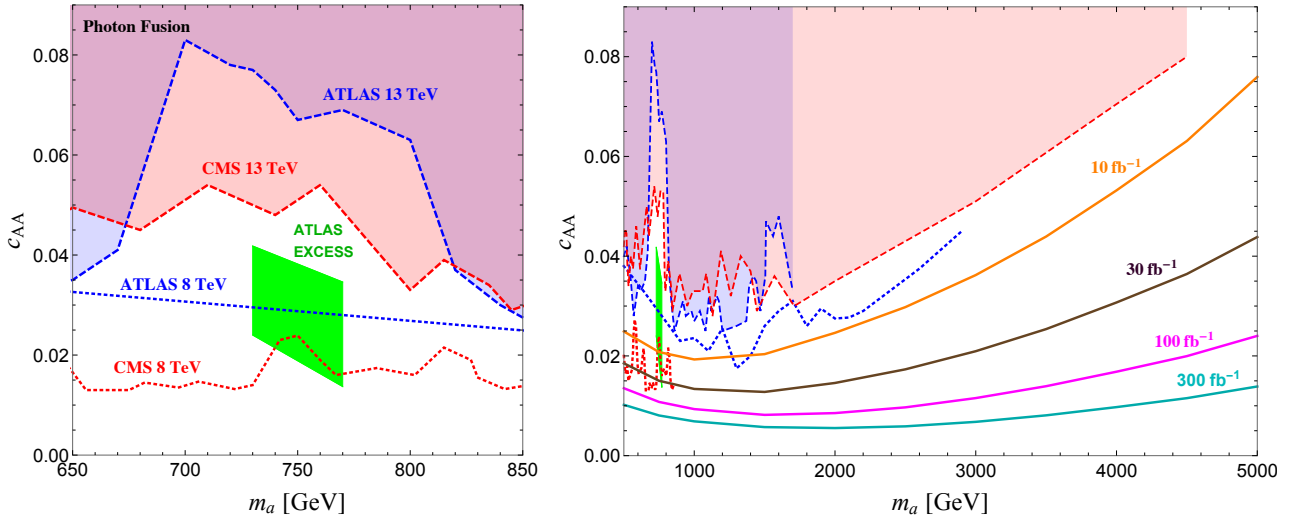


FIG. 2. LHC constraints and expected future reach of the diphoton channel in the plane (m_a, c_{AA}) . We assume that a is totally produced by photon fusion and decays to $\gamma\gamma$ with a branching ratio equal to 0.6. *Left plot*: ATLAS excess plus LHC-8 and LHC-13 constraints for searches for diphoton resonances in the mass region near 750 GeV. *Right plot*: LHC constraints and expected 2σ LHC-13 reach for different integrated luminosities: 10, 30, 100, 300 fb^{-1} . See the text for details.

parameters fitting the central value of the ATLAS excess within $\pm 1\sigma$. We use the 730 and 770 GeV bins of the ATLAS data [3]. With the assumed value of $\text{BR}(a \rightarrow \gamma\gamma)$ we find that the required $c_{AA} \approx 0.03$ corresponds to a $\Lambda_{\text{NP}} \approx 650$ GeV. This naive estimate suggests the existence of a new physics scale consistent with minimal models of dynamical EW symmetry breaking, that we will explore in the next section.

We now turn our attention to LHC-8 earlier constraints and confront them with the LHC-13 results. The dotted and dashed curves in Fig. 2 are respectively the LHC-8 and LHC-13 constraints from searches tailored for diphoton resonances. The curves are obtained using the 95% C.L. limits given in [3] ([54]), which refer to the 13 (8) TeV ATLAS data at 3.2 (20.3) fb^{-1} , and in [4] ([55]) for the 13 (8) TeV CMS data with 2.6 (19.7) fb^{-1} . We present only the CMS results associated with the narrow-width scenario, which is appropriated for the photon fusion production.

One observes a slight tension with respect to the 8 TeV data, in particular with those from CMS. Taking into account the uncertainty on the photon fusion production cross section which is about 50% [49], reduces this tension below the 1σ level (see also [14] for a recent discussion).

Beyond the excess at 750 GeV it is interesting to explore the LHC-13 reach of the diphoton channel for larger masses of the new pseudoscalar state. We therefore need to estimate the background. As proved in [3, 4] a functional form provides a good description of the background. We thus adopt the same estimate of the ATLAS analysis [3], which yields the following best-fit curve for the number of background events as function of the invariant mass $m_{\gamma\gamma}$:

$$B(x, L) = \frac{L}{3.2 \text{ fb}^{-1}} \left(1 - x^{1/3}\right)^{9.9} x^{-2.3} \quad (11)$$

with $x = m_{\gamma\gamma}/\sqrt{s}$ and L being the total integrated luminosity. We then estimate the reach by applying the same ATLAS selection criteria in [3] according to which the transverse energies ($E_T^{\gamma_{1,2}}$) and the pseudo-rapidity (η_γ) of the two leading photons must satisfy

$$E_T^{\gamma_1} > 0.4 m_{\gamma\gamma}, \quad E_T^{\gamma_2} > 0.3 m_{\gamma\gamma}, \quad |\eta_\gamma| < 2.37 \quad (|\eta_\gamma| \notin [1.37, 1.52]). \quad (12)$$

Furthermore, the photons must be isolated following

$$E_T^{\text{iso}} < 0.05 E_T^{\gamma_{1,2}} + 6 \text{ GeV}, \quad (13)$$

where E_T^{iso} is defined as the transverse energy of the vector sum of all stable particles found within a cone $\Delta R \leq 0.4$ around the photon, neglecting muons and neutrinos. Finally, we assume a 95% efficiency for the photon identification.

We simulate the signal with Madgraph5 [48], passing the events to PYTHIA [56] for showering and hadronization and to Delphes3 [57] to mimic detector effects. We use the ATLAS default detector card with the isolation criteria reported in (13). After applying the selection cuts above, we obtain signal acceptances from 0.47 for $m_a = 0.5$ TeV to 0.56 for $m_a = 5$ TeV. The reach is then estimated by assuming a sensitivity $S/\sqrt{S+B} = 2$, where S (B) represents the number of signal (background) events at a given integrated luminosity, which pass the selection. This gives a conservative estimate of 95% C.L. limits that LHC-13 will be able to place at different luminosities. The results of this analysis are illustrated in the right plot of Fig. 2. As anticipated they can be applied to any model with a pseudoscalar particle entirely produced via photon fusion and where no new decay channels open at higher energies. For example, models featuring an effective photon coupling in the range $0.015 \lesssim c_{AA} \lesssim 0.04$ suggested by the excess, can be ruled out for a masses up to around 2.5, 4 and more than 5 TeV with respectively 10, 30 and 100 fb^{-1} of collected integrated luminosity at the LHC-13. We also observe that the 8 TeV searches [54, 55] put so far the strongest constraints, with ATLAS reaching $m_a = 2.9$ TeV. Intriguingly, the LHC-8 analysis performed by ATLAS is even compatible with another excess around $m_a = 1.6$ TeV from the LHC-13 run corresponding to a local significance of about 2.8σ . The latter could be excluded in the upcoming run with circa 10 fb^{-1} , shown as the orange curve in the plot.

Summarizing the results for the photon fusion production mechanism, we have shown that LHC-13 can test the presence of new pseudoscalar states up to several TeVs. More precise limits can be obtained, following our analysis, once the photon PDFs will be known more accurately.

B. Production via top-mediated gluon fusion: broadening the resonance

We now turn on the coupling y_t to the top, see (1), and show that it is possible to fit the 750 GeV diphoton excess while simultaneously accommodating a wide total width $\Gamma_{\text{tot}}(a) \approx 45$ GeV ($\Gamma_{\text{tot}}(a)/m_a \approx 0.06$), currently preferred by ATLAS. Indeed, in this case $\Gamma_{\text{tot}}(a)$ is dominated by the tree-level decay of a into a $t\bar{t}$ pair, see (9). Of course, the production of a relies on the top-mediated gluon fusion mechanism yielding the signal cross section

$$\sigma(pp \rightarrow a \rightarrow \gamma\gamma) = \frac{\pi^2 \Gamma(a \rightarrow gg)}{8 m_a} \frac{d\mathcal{L}^{gg}}{dm_a^2} \times \text{BR}(a \rightarrow \gamma\gamma), \quad (14)$$

where $\Gamma(a \rightarrow gg) \propto y_t^2$ and $d\mathcal{L}^{gg}/dm_a^2$ is the gluon luminosity function, which can be read from Fig. 1. Notice that if $\Gamma_{\text{tot}}(a) \simeq \Gamma(a \rightarrow t\bar{t}) \propto y_t^2$ the cross section (10) simplifies to

$$\sigma(pp \rightarrow a \rightarrow \gamma\gamma) \simeq c_{AA}^2 \frac{\alpha_S^2 |F(m_a^2/4m_t^2)|^2}{6144 \pi} \frac{m_a^4}{m_t^2 v^2} \frac{d\mathcal{L}^{gg}}{dm_a^2}, \quad (15)$$

it does not depend on y_t and it is controlled by the effective coupling c_{AA} .

Using (14) we start by considering the case of a fixed $\text{BR}(a \rightarrow \gamma\gamma) = 0.01$ and determine the range of y_t compatible with the 750 GeV excess. The best fit region for a wide-width resonance must reproduce simultaneously the two bins in the diphoton invariant mass at 730 and 770 GeV [3]. This gives the green band shown in the left plot of Fig. 3, according to which $0.94 \lesssim y_t \lesssim 1.25$. The blue dashed (dotted) curve in the plot represents the 95% C.L. limits in [3] ([54]) for the 13 (8) TeV ATLAS data with 3.2 (20.3) fb^{-1} . Analogously, the red lines show the CMS bounds [4] ([55]) for a wide-width resonance at 13 (8) TeV and 2.6 (19.7) fb^{-1} . Part of the parameter space is also excluded by $t\bar{t}$ resonance searches. So far the strongest constraints on these resonances are set by the combined CMS analyses in different $t\bar{t}$ final states at LHC-8 with 19.7 fb^{-1} [58]. Such limits are indicated by the black dot-dashed line in the figure ³. We also checked that the searches for di-jet resonances [59–62] do not place any bound on the relevant parameter space. In contrast to the photon fusion scenario, where the resonance is narrow, now there is no significant tension between the 8 TeV results and the ATLAS diphoton excess. We also verify that for $\text{BR}(a \rightarrow \gamma\gamma) = 0.01$ the values of y_t that reproduce the diphoton excess imply a total width in the range $35 \text{ GeV} \lesssim \Gamma_{\text{tot}}(a) \lesssim 62 \text{ GeV}$. On the other hand, taking $y_t = 1$, the same range of $\Gamma_{\text{tot}}(a)$ is obtained for $\text{BR}(a \rightarrow \gamma\gamma)$ between 0.009 and 0.016. Henceforth, we conclude that only models predicting $y_t \approx 1$ and $\text{BR}(a \rightarrow \gamma\gamma) \approx 0.01$ can reproduce the ATLAS best-fit of the diphoton invariant mass.

Under the assumption that the total width is dominated by the $t\bar{t}$ decay rate, as argued before, the cross section does not depend on y_t . We can therefore use (15) to study the LHC-13 reach/constraints of the diphoton channel on

³ More precisely, we use the limits in [58] for a Z' decaying into $t\bar{t}$ with a width-over-mass ratio of 0.1.

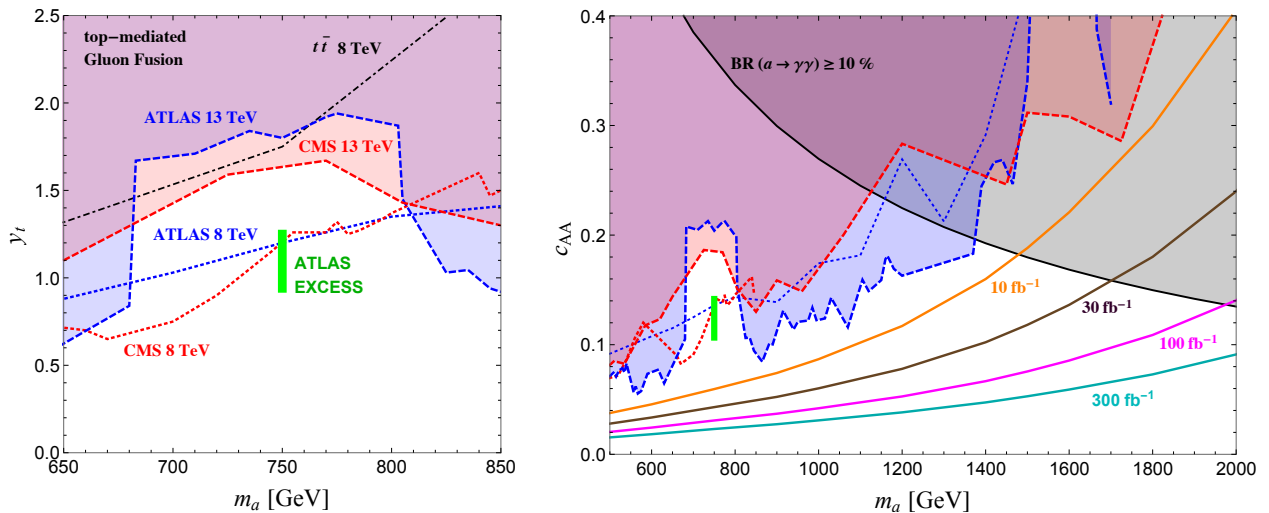


FIG. 3. LHC constraints and expected future reach of the diphoton channel in the planes (m_a, y_t) (left plot) and (m_a, c_{AA}) (right plot). We assume that a is totally produced by top-mediated gluon fusion. *Left plot:* ATLAS excess plus LHC-8 and LHC-13 constraints from searches for diphoton and $t\bar{t}$ resonances in the mass region near 750 GeV. We assume $\text{BR}(a \rightarrow \gamma\gamma) = 1\%$. *Right plot:* LHC constraints and expected 2σ LHC-13 reach for different integrated luminosities: 10, 30, 100, 300 fb^{-1} , under the assumption that $\Gamma_{\text{tot}}(a) \simeq \Gamma(a \rightarrow t\bar{t})$. The dark shaded area corresponds to $\text{BR}(a \rightarrow \gamma\gamma) \geq 10\%$ and is indicative of a region of the parameter space where relevant corrections to our predictions may apply. See text for details.

the (m_a, c_{AA}) plane, as done for the photon fusion production. We estimate the background according to (11) and we apply the cuts in (12, 13) to the signal events simulated with Madgraph5+PYTHIA+Delphes3. Note that the gluon fusion production includes the NLO K-factors discussed in section II. We obtain signal acceptances from 0.43 at $m_a = 0.5$ TeV to 0.46 at 2 TeV. The limits we obtain from this analysis are shown on the right plot of Fig. 3. We observe that the values of c_{AA} that can explain the ATLAS excess at 750 GeV lay in the interval $0.10 \lesssim c_{AA} \lesssim 0.14$. These are larger than in the photon fusion case by a factor around 3. Any model with values of c_{AA} in this range and for which $\Gamma_{\text{tot}}(a) \simeq \Gamma(a \rightarrow t\bar{t})$ can be ruled out up to $m_a = 1.3, 1.6$ and 2 TeV with respectively 10, 30, and 100 fb^{-1} at LHC-13. Furthermore, we observe that, in contrast to the photon fusion scenario shown in Fig. 2, the current strongest constraints are now set by the 13 TeV ATLAS data rather than the LHC-8 results. This depends on the larger increase of the gluon PDF, compared to the photon PDF, passing from $\sqrt{s} = 8$ TeV to $\sqrt{s} = 13$ TeV.

Finally, the gray-shaded area in the plot indicates the region of the parameter space where the $\text{BR}(a \rightarrow \gamma\gamma)$ is larger than 10% (calculated for $y_t = 1$). Above this value, corrections to the approximated expression for the cross section in (15) become relevant and we further expect non negligible contributions to the production cross section from photon fusion.

We briefly summarize the salient results presented in this section. We have learned that: i) it is possible to directly photo-produce the 750 GeV excess without the need of any colored state; ii) in this case the resonance is narrow; iii) beyond the 750 GeV excess LHC-13 will be able to constrain new resonances up to 5 TeV with 100 fb^{-1} ; iv) a broad width for the 750 GeV excess can be minimally achieved when the new resonance couples to the SM top with a perturbative Yukawa-like coupling; v) the reach in this case is around 2 TeV for 100 fb^{-1} .

We now move to a concrete realization of these scenarios in terms of minimal models of composite dynamics.

III. DIPHOTON RESONANCES IN SCENARIOS OF MINIMAL COMPOSITE DYNAMICS

We consider now a UV completion of the effective field theory introduced in section II. The theory naturally predicts a new pseudoscalar particle in the TeV range that can be revealed by LHC searches for diphoton resonances. This is realized in a minimal framework of composite dynamics naturally addressing the SM hierarchy problem. The model includes N_F new fermions, hereafter dubbed techniquarks, which engage in a new (asymptotically free) $SU(N_T)$ gauge interaction. For massless techniquarks transforming in a complex representation of the underlying gauge composite theory, and in absence of EW interactions, the theory preserves an $SU(N_F)_L \times SU(N_F)_R$ global

chiral symmetry which spontaneously breaks around $\Lambda_T \gtrsim 1$ TeV to the custodial group $SU(N_F)_V$. A larger global quantum symmetry occurs when the underlying fermions belong to a (pseudo)real representation of the fundamental composite gauge group, i.e. $SU(2N_F)$. Enlarged global symmetries are interesting since they lead to composite pseudo-Goldstone Higgs realizations [63, 64].

The $N_F^2 - 1$ Goldstone bosons which arise from the breaking of the axial-vector symmetry are, therefore, massless composite pseudoscalar fields made up of the new fermions and their antiparticles. It is customary to describe them, as well as possible new pseudoscalar isosinglets of flavor, by a $N_F \times N_F$ unitary matrix \mathcal{U} , which transforms bilinearly under a chiral rotation:

$$\mathcal{U} \rightarrow u_L \mathcal{U} u_R^\dagger \quad (16)$$

with $u_{L/R} \in SU(N_F)_{L/R}$. When the EW $SU(2)_W \times U(1)_Y$ gauge interactions are switched on, three of the Goldstone bosons become the longitudinal degrees of freedom of the W^\pm and Z gauge bosons, while the photon remains massless.

In the following we consider for simplicity an underlying theory with $N_F = 2$ techniquarks U and D , which transform under a given complex representation R of the new gauge group. Furthermore, within this minimal composite scenario, we assume that U and D do not carry SM color, i.e. they are singlet of $SU(3)_C$. On the other hand, the left-handed and right-handed chiral projections of the new fundamental fermions have non-trivial quantum numbers under the EW gauge symmetry. In order to cancel Witten [65] and gauge anomalies we further enlarge the fermion sector with new leptons, N and E , with proper weak gauge and hypercharge quantum numbers [66]. In particular, the left-handed projections $Q_L \equiv (U_L, D_L)$ and $L_L \equiv (N_L, E_L)$ transform in the fundamental of $SU(2)_W$, while the corresponding right-handed fields U_R, D_R, N_R and E_R are weak isosinglets. The hypercharge assignments which make the theory anomaly free are

$$\begin{aligned} Y(Q_L) &= \frac{y}{2}, & Y(U_R/D_R) &= \frac{y \pm 1}{2}, \\ Y(L_L) &= -3 \frac{y}{2} & Y(N_R/E_R) &= \frac{-3y \pm 1}{2}, \end{aligned} \quad (17)$$

where y is a real parameter. The electric charge operator is defined as $Q = T_3 + Y$, where T_3 is the weak isospin generator. In the following, we will assume the new leptons to be sufficiently heavy not to affect our results⁴.

The condensation of the techniquarks, i.e. $\langle 0 | \bar{U}U + \bar{D}D | 0 \rangle \neq 0$, induces the chiral symmetry breaking pattern $SU(2)_L \times SU(2)_R \rightarrow SU(2)_V$, as well as the correct breaking of the EW symmetry. The latter is embedded by gauging a subgroup of $SU(2)_L \times SU(2)_R \times U(1)_V$. The spectrum of the massive states depends sensitively on the specific underlying dynamics. In QCD-like theories we expect new resonances to appear at energy scales around Λ_T as further confirmed by recent lattice simulations [68, 69]⁵. If, however, the dynamics is not QCD-like the spectrum can be much more compressed [81, 82] and furthermore the top-interactions can, via quantum effects, further reduce the lightest scalar mass [82]. Analytical [83–85] and numerical efforts [86–94] have been dedicated to determine whether fermionic gauge theories display large distance conformality and investigate their spectrum. For the sextet composite model [81, 83, 95], lattice results [96–98] suggest that the theory is either very near-conformal or conformal. In the latter case interactions responsible for giving masses to the SM fermions can modify the conformal-boundary inducing an ideal near-conformal behaviour [99]. Furthermore, near-conformality alleviates tension with EW precision measurements [100] and flavor changing neutral current constraints [101].

An interesting state is the pseudoscalar a associated with the $U(1)_A$ axial anomaly of the underlying gauge theory, which is analogous to the η' of QCD. This is the one we assume to induce the diphoton excess and it is included as a singlet state in the matrix \mathcal{U} . The pseudoscalar degrees of freedom are therefore parametrized via the following unitary matrix \mathcal{U} transforming as in (16) for $N_F = 2$, that is

$$\mathcal{U} = e^{i\Phi/F_T} = \exp \left[\frac{i}{F_T} (a + \boldsymbol{\tau} \cdot \boldsymbol{\Pi}) \right], \quad (18)$$

where $\boldsymbol{\tau} \equiv (\tau_1, \tau_2, \tau_3)$ are the standard Pauli matrices. The technipions $\boldsymbol{\Pi} \equiv (\Pi^1, \Pi^2, \Pi^3)$ couple with strength F_T to the axial-currents corresponding to the broken generators of the chiral symmetry. The linear combinations $\Pi^\pm \equiv (\tau_1 \mp i\tau_2)/\sqrt{2}$ and $\Pi^0 \equiv \Pi_3$ become the longitudinal polarizations of the W^\pm and the Z bosons, respectively, which thus acquire masses

$$m_W^2 = \frac{1}{2} g_W F_T^2, \quad m_Z^2 = \frac{1}{2} \sqrt{g_W^2 + g_Y^2} F_T^2, \quad (19)$$

⁴ The current direct limit on the mass of heavy charged leptons is about 574 GeV [67] for stable singly-charged particles.

⁵ Recently also the vector decay constants [70] have been computed for the minimal composite template that can be used for technicolor, composite Goldstone Higgs, and even models of strongly interacting massive particles for dark matter of either asymmetric [71–77] or mixed nature [78], or that can reach the observed relic density via three to two number changing interactions [79, 80].

with $F_T = v = 246$ GeV.

Heavy vector mesons are also generated by the composite dynamics. The relevant states here are given by one isosinglet (ω) and one isotriplet (ρ) spin-1 resonance, which is described by the matrix

$$\mathcal{V}^\mu = \lambda (\omega^\mu + \boldsymbol{\tau} \cdot \boldsymbol{\rho}^\mu), \quad (20)$$

where λ is a parameter connected to the ρ -II-II effective coupling. These new vector mesons have typically masses of the order of a few TeVs [68–70]. In this case, their mixing with the technipions, namely the EW gauge bosons, which could in principle have an impact on the decays of a , can be safely neglected. Furthermore, since this study will be focused on the phenomenology of the pseudoscalar meson, we will assume in the following that the vectors are decoupled. A specific study of collider signatures of composite vector mesons that might be lighter because of near-conformal dynamics is very interesting and will be presented elsewhere.

The low energy physics below the composite scale Λ_T is encoded in the following effective Lagrangian \mathcal{L}_{eff} constructed to respect all the symmetries of the underlying theory. Neglecting gauge fixing and Faddeev-Popov terms, the skeleton of the effective Lagrangian reads:

$$\mathcal{L}_{\text{eff}} = -\frac{1}{4} B^{\mu\nu} B_{\mu\nu} - \frac{1}{4} \text{Tr} [W^{\mu\nu} W_{\mu\nu}] + \mathcal{L}_{\text{comp}} + \mathcal{L}_{\text{ferm}}, \quad (21)$$

where $B^{\mu\nu}$ and $W^{\mu\nu}$ are the field strengths of the EW gauge bosons. Here the techniquarks and the $SU(N_T)$ gauge fields are integrated out, while the SM fermions and the new leptons N and E are coupled to the composite states via $SU(2)_W \times U(1)_Y$ invariant operators in $\mathcal{L}_{\text{ferm}}$, which originates from an unspecified extended gauge dynamics (EGD). The details of the underlying theory are encoded in the effective parameters of \mathcal{L}_{eff} . The measurement of some of them in current and future collider experiments will allow to infer more insights about the new strong dynamics that can be confronted with first principle lattice predictions. Here we point out the importance of searches for diphoton resonances. In fact, in our theory the composite meson a can be naturally identified with the particle responsible for local excess in the diphoton invariant mass at 750 GeV.

The Lagrangian $\mathcal{L}_{\text{comp}}$ in (21) contains the gauge invariant effective interactions involving \mathcal{U} . In particular, the leading terms are:

$$\mathcal{L}_{\text{comp}} = \frac{1}{4} F_T^2 \text{Tr} \left[(\mathcal{D}^\mu \mathcal{U})^\dagger \mathcal{D}_\mu \mathcal{U} \right] + \mathcal{L}_{m_a} + \mathcal{L}_{\text{WZW}} + \dots \quad (22)$$

The covariant derivative in (22) takes the standard form

$$\mathcal{D}^\mu \mathcal{U} = \partial^\mu \mathcal{U} - i A_L^\mu \mathcal{U} + i \mathcal{U} A_R^\mu, \quad (23)$$

with

$$A_L^\mu = g_Y \left(Q - \frac{1}{2} \tau_3 \right) B^\mu + \frac{1}{2} g_W \boldsymbol{\tau} \cdot \mathbf{W}^\mu, \quad A_R^\mu = g_Y Q B^\mu, \quad (24)$$

where Q is the electric charge matrix of the fundamental techniquarks. Under $SU(2)_W \times U(1)_Y$ gauge transformations

$$A_L^\mu \rightarrow u_L A_L^\mu u_L^\dagger - i \partial_\mu u_L u_L^\dagger, \quad A_R^\mu \rightarrow u_R A_R^\mu u_R^\dagger - i \partial_\mu u_R u_R^\dagger. \quad (25)$$

where $u_L \in SU(2)_W$ and $u_R \equiv \exp(i\theta(x)\tau_3/2)$. Notice that the matrix \mathcal{U} is not sensitive to the hypercharge parameter y , because it is formed by pairs made by a techniquark and the corresponding antiparticle, see (17).

The physical masses of the EW gauge bosons in (19) arise directly from the first operator in (22), whereas \mathcal{L}_{m_a} provides a mass term for a . Taking the techniquarks in the fundamental representation, $d(R = \text{Fund}) = N_T$, the corresponding gauge invariant Lagrangian is

$$\mathcal{L}_{m_a} = \frac{1}{32} m_a^2 F_T^2 \text{Tr} [\ln \mathcal{U} - \ln \mathcal{U}^\dagger]^2, \quad (26)$$

where the mass m_a is given at leading order in the large N_T limit by the Witten-Veneziano relation [102, 103]

$$m_a = \sqrt{\frac{2}{3}} \frac{F_T}{f_\pi} \frac{3}{N_T} m_{\eta_0} \approx \frac{6}{N_T} \text{TeV}. \quad (27)$$

Here $f_\pi = 92$ MeV is the pion decay constant and $m_{\eta_0} = 849$ MeV. η_0 indicates the QCD $SU(3)$ flavor singlet state in the chiral limit with $m_{\eta_0}^2 = m_{\eta'}^2 + m_\eta^2 - 2m_K^2$. As we can see from (27), for techniquarks in the fundamental

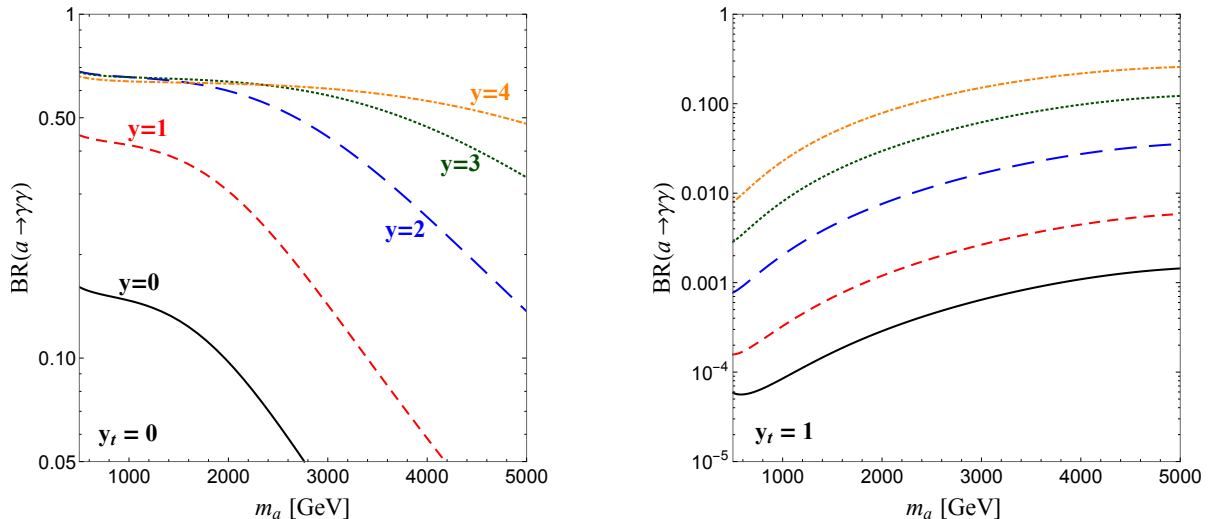


FIG. 4. Branching ratio into two photons of the pseudoscalar a as a function of its mass for several values of the hypercharge parameter y . The scenario without (with) a direct coupling to the top quark, $y_t = 0$ ($y_t = 1$), corresponds to a narrow (wide) resonance for $m_a = 750$ GeV. See the text for details.

representation of the new gauge interaction we naturally expect values of the pseudoscalar mass in the TeV range. This is actually also the case for different representations [104, 105], for which expression (27) cannot be applied. In our numerical analysis we will fix $d(R) = 6$.

The gauged Wess-Zumino-Witten Lagrangian \mathcal{L}_{WZW} is a topological term stemming from chiral anomalies associated with the global axial-vector currents. The complete expression of such term is reported in (A2) and parametrizes EW processes which can be directly tested at the LHC. In particular, we are interested here in the production mechanisms of the a resonance at LHC and its decays into EW gauge bosons via the relevant topological terms. We have at leading order in the derivative expansion of the theory

$$\begin{aligned} \mathcal{L}_{\text{WZW}} = & -\frac{i5C}{F_T} \epsilon_{\mu\nu\rho\sigma} \text{Tr} [\Phi (\partial^\mu A_L^\nu \partial^\rho A_L^\sigma + \partial^\mu A_R^\nu \partial^\rho A_R^\sigma + \partial^\mu (A_L^\nu + A_R^\nu) \partial^\rho (A_L^\sigma + A_R^\sigma))] \\ & + \frac{5C}{F_T^3} \epsilon_{\mu\nu\rho\sigma} \text{Tr} [\partial^\mu \Phi \partial^\nu \Phi \partial^\rho \Phi (A_L^\sigma + A_R^\sigma)] + \dots, \end{aligned} \quad (28)$$

with $C = -id(R)/(240\pi^2)$. The matching between (28) and the effective Lagrangian in (1) gives the following effective couplings:

$$\begin{aligned} c_{AA} &= (1+y^2) e^2 \frac{d(R)}{8\pi^2}, & c_{AZ} &= \frac{1-2(1+y^2)s_W^2}{2c_W s_W} e^2 \frac{d(R)}{8\pi^2}, \\ c_{ZZ} &= e^2 \frac{1-3s_W^2+3(1+y^2)s_W^4}{3c_W^2 s_W^2} \frac{d(R)}{8\pi^2}, & c_{WW} &= e^2 \frac{1}{s_W^2} \frac{d(R)}{24\pi^2}. \end{aligned} \quad (29)$$

The second term in (28) mediates the three-body decay process $a \rightarrow \Pi \Pi V$, where V is one EW transverse gauge boson, $V = \gamma/Z/W^\pm$, and Π are the longitudinal components of Z/W^\pm . In the limit $m_{\Pi^\pm} \approx m_{\Pi^0} \equiv m_\Pi$, the three-body partial decay rate of a reads

$$\begin{aligned} \Gamma(a \rightarrow \Pi \Pi V) = & \frac{m_a^3}{122880\pi^3} \frac{m_a^4}{F_T^6} \left[\sqrt{1-4u^2} (1-2u^2 (14+47u^2-80u^4+60u^6)) \right. \\ & \left. + 240u^4 (-1+2u^2-3u^4+2u^6) \ln \left(\frac{2u}{1+\sqrt{1-4u^2}} \right) \right] c_{\Pi\Pi V}^2, \end{aligned} \quad (30)$$

y	0	1	2	3	4
$\Gamma_{\text{tot}}(a)$ [MeV]	13	18	73	290	870
$\Gamma(a \rightarrow \gamma\gamma)$ [MeV]	1.9	7.7	48	190	560
$\Gamma(a \rightarrow \gamma Z)$ [MeV]	1.5	0.030	8.9	68	240
$\Gamma(a \rightarrow ZZ)$ [MeV]	1.4	2.4	7.7	23	57
$\Gamma(a \rightarrow W^+W^-)$ [MeV]	7.5				
$\Gamma(a \rightarrow 3\text{-body})$ [MeV]	0.10				

TABLE I. Total and partial decay widths from the WZW term in (28) for a narrow pseudoscalar resonance of mass $m_a = 750$ GeV as a function of the hypercharge of the fundamental techniquarks. We fix the dimension of the techniquark representation to $d(R) = 6$.

where $u \equiv m_\Pi/m_a$ and

$$c_{\Pi^+\Pi^-\gamma} = e \frac{d(R)}{12\pi^2}, \quad c_{\Pi^+\Pi^-Z} = \frac{1 - 2s_W^2}{2c_W s_W} c_{\Pi^+\Pi^-\gamma}, \quad c_{\Pi^\pm\Pi^0W^\pm} = \pm \frac{1}{2s_W} c_{\Pi^+\Pi^-\gamma}. \quad (31)$$

A. WZW induced photon fusion production

Having spelled out the underlying dynamics and provided the associated effective Lagrangian, we can now turn to the diphoton process. We first analyse the most minimal case in which the gauged WZW term is simultaneously responsible for the production of a and its decay into photons. This allows us to provide critical information on the decay rates (and production) of a in several related channels when compared to the blind effective approach used in the previous section. In table I we report the total decay rate $\Gamma_{\text{tot}}(a)$ and the partial widths of a into EW gauge bosons for $m_a = 750$ GeV and different choices of the techniquark parameter y . Notice that for this value of the mass the diphoton resonance is quite narrow, which seems to be preferred by the CMS results [4]. The diphoton decay channel dominates the total width for a non-zero value of the parameter y entering the hypercharge assignment (17). These results have been obtained in [5] with the important difference that in that work the production mechanism was induced by a new vector-like colored fermion with a mass around one TeV.

From the table we observe that there is a strong suppression in the production of one photon and one Z for $y \approx 1$, due to the cancellation in the expression of the effective coupling c_{AZ} . As for the ZZ and WW channels, they are subdominant for $y > 1$. On the other hand, the three-body decay from (30), which is negligible for $m_a = 750$ GeV, may have a relevant contribution in the total decay rate for larger masses, i.e. $m_a \gtrsim 1.5$ TeV, because the corresponding partial decay width increases $\propto m_a^7$. This is manifest in the left panel of Fig. 4, which shows the branching ratio of a decaying into two photons versus m_a , for fixed values of y . In the case of $y \gtrsim 2$ and $m_a \lesssim 2$ TeV the diphoton decay rate is anyway the largest one.

The constraints on the effective coupling to the photons c_{AA} as well as the values of the parameters explaining the ATLAS excess, reported in Fig. 2, can be directly interpreted in the plane (m_a, y) for $m_a \lesssim 2$ TeV, where the effect of the three-body decays is negligible and $\text{BR}(a \rightarrow \gamma\gamma)$ is independent of m_a , see (5-8) and the left plot in Fig. 4. Our results are shown in Fig. 5, where the dashed (dotted) curves represent the ATLAS and CMS limits at 13 (8) TeV as in Fig. 2, and the green area indicates the interval $0.9 \lesssim y \lesssim 2.1$ which fits the ATLAS data at $m_a = 750$ GeV. For this range of the hypercharge one finds $0.4 \lesssim \text{BR}(a \rightarrow \gamma\gamma) \lesssim 0.7$. Hence, we compute the LHC-13 future constraints on y , following the analysis done in subsection II A, where we include the variation in the diphoton branching ratio due to the three-body decay channels. In conclusion, we find that it is possible to probe values of y as small as 0.6 with a luminosity of 300 fb^{-1} at LHC-13.

B. Top-mediated gluon fusion and WZW induced diphoton decay

Now we turn to a more general realization in which we allow for direct couplings of a to the SM fermions. These may be originated by the same EGD responsible for the generations of the fermion masses. Independently of the underlying theory, such interactions are parametrized at low energy by gauge invariant effective operators included in

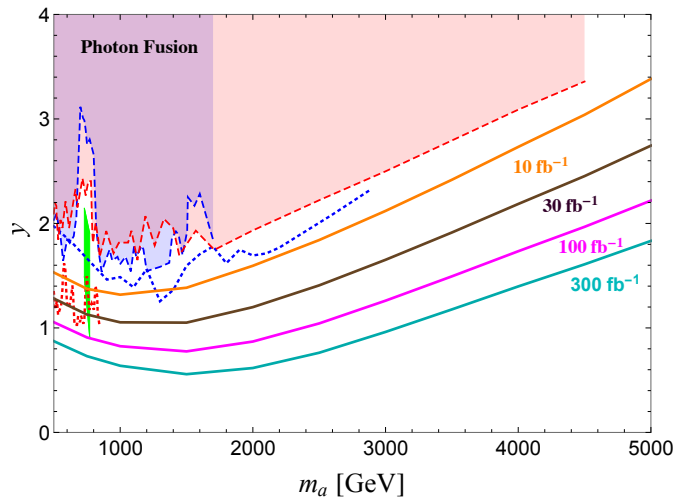


FIG. 5. LHC constraints, 750 GeV ATLAS excess and expected LHC-13 future reach of the diphoton channel in the plane (m_a, y) . Here a is totally produced by photon fusion. We fix the dimension of the techniquark representation to $d(R) = 6$. The plot legend is the same as in Fig. 2.

$\mathcal{L}_{\text{ferm}}$ of (21). We expect, as for the Higgs boson h , the strongest interactions to arise for the third quark generation. Indeed, indicating the top and bottom quark mass eigenstates with $Q_3 \equiv (t, b)^T$, their embedding in $\mathcal{L}_{\text{ferm}}$ is given by the $SU(2)_W \times U(1)_Y$ invariant effective operators

$$\begin{aligned} \mathcal{L}_{\text{ferm}} = & i \bar{Q}_{3L} \gamma_\mu (\partial^\mu - i A_L^\mu) Q_{3L} + i \bar{Q}_{3R} \gamma_\mu (\partial^\mu - i A_R^\mu) Q_{3R} \\ & - Y_1 F_T f_1(h) (\bar{Q}_{3L} \mathcal{U} Q_{3R} + \bar{Q}_{3R} \mathcal{U}^\dagger Q_{3L}) - Y_2 F_T f_2(h) (\bar{Q}_{3L} \mathcal{U} \tau_3 Q_{3R} + \bar{Q}_{3R} \tau_3 \mathcal{U}^\dagger Q_{3L}) + \dots \end{aligned} \quad (32)$$

where $Q_{3L/R} = P_{L/R} Q_3$ and $P_{L/R} = (\mathbf{1} \mp \gamma_5)/2$ are the chiral projectors. At leading order in h/F_T the functions $f_{1,2}(h)$ are

$$f_{1,2}(h) = 1 + c_{1,2} \frac{h}{F_T} + \dots \quad (33)$$

The coefficients $c_{1,2}$ are constrained by measurements of the Higgs couplings to the SM fermions [106], whereas $Y_{1,2}$ reproduce the top and bottom masses: $m_t = (Y_1 + Y_2) F_T$ and $m_b = (Y_1 - Y_2) F_T$. From (32) we get the following effective couplings between a and the third quark generation

$$\mathcal{L}_{\text{ferm}} \supset -\frac{m_t}{F_T} i a \bar{t} \gamma_5 t - \frac{m_b}{F_T} i a \bar{b} \gamma_5 b, \quad (34)$$

which for $F_T = v$ predicts the effective coupling to the top $y_t = 1$ in the effective Lagrangian (1). The Yukawa-like terms in (32), at the underlying level, originate from effective four-fermion type interactions involving two techniquarks and two SM fermions. This scenario belongs to the class of models discussed in subsection II B, where the diphoton resonance is wide and it is produced via top-mediated gluon fusion. Furthermore we can neglect the extra top-mediated contributions to the effective coefficients c_{VV} to the EW gauge bosons, since they are subdominant compared to the gauged WZW terms given in (29).

We report in the right plot of Fig. 4, the $\text{BR}(a \rightarrow \gamma\gamma)$ versus m_a in the case the pseudoscalar resonance a is coupled to the SM third generation according to (34), for $d(R) = 6$ and different values of the techniquark hypercharge parameter y . The resulting total width for $m_a = 750$ GeV is $\Gamma_{\text{tot}}(a) \approx 40$ GeV, which is in remarkable agreement with the wide-width scenario reported by the ATLAS collaboration [3]. In this case, taking $3.6 \lesssim y \lesssim 4.1$, it is possible to reproduce the diphoton excess⁶. For values of the hypercharge parameter $y \approx 4$ the diphoton branching ratio is of the order of 1% at $m_a = 750$ GeV. This implies that our scenario is consistent with the ATLAS best-fit of the

⁶ When the heavy charged leptons, E and N , have masses above $m_a/2$ and couple to a like the SM fermions, we checked that their contribution enhances the a diphoton branching ratio in such a way that the y reproducing the excess is around 3. Notice that in the case the pseudoscalar resonance is also coupled to a heavy vector-like quark, the gluon fusion production cross section can be further enhanced reproducing the ATLAS excess at 750 GeV for even smaller values of y [5].

diphoton invariant mass, as discussed in subsection IIB and shown explicitly in the left plot of Fig. 3. Similarly, the right plot of Fig. 3 can be directly used to estimate the LHC-13 reach on the (m_a, y) parameter space. In particular, we can see that with a luminosity of 100 fb^{-1} it is possible to test scenarios with $\text{BR}(a \rightarrow \gamma\gamma) \lesssim 10\%$ ($y \lesssim 4$) up to $m_a \approx 2 \text{ TeV}$.

IV. CONCLUSIONS

The diphoton channel is becoming increasingly attractive in spotting or constraining new physics at the LHC. Further inspired by the tantalizing excess at 750 GeV we analyzed the reach of this channel first via an effective operator approach and then for minimal models of dynamical electroweak symmetry breaking.

From our general effective analysis we deduced that it is possible to directly photo-produce the 750 GeV resonance without the need of any colored state and that in this case the resonance is narrow. Beyond the 750 GeV excess, we have demonstrated that LHC-13 will constrain new diphoton resonances up to a wide energy range reaching circa 5 TeV with 100 fb^{-1} , as shown in Fig. 2. We also noted that a broad width for the 750 GeV resonance can be minimally achieved via a perturbative Yukawa-like coupling to the Standard Model top. In this case the resonance is produced via top-mediated gluon fusion and we showed in Fig. 3 that the LHC reach is around 2 TeV for 100 fb^{-1} .

In the second part of the paper we introduced minimal models of composite dynamics. Here the diphoton channel stems from the topological sector of the theory and can account for the experimental excess. The relevant composite state is the pseudoscalar associated with the axial anomaly of the new underlying dynamics. We independently analyzed the photon and the top-mediated gluon fusion production mechanisms and in both cases we determined the corresponding LHC reach. In the case of photon fusion we found that with 100 fb^{-1} LHC-13 can probe values of the techniquark hypercharge parameter, defined in (17), as small as $y \approx 0.8$, as shown in Fig. 5. For the top-mediated gluon fusion one can adopt the constraints found in the effective approach analysis, by using the matching relations in (29). In this case we obtained that with a luminosity of 100 fb^{-1} LHC-13 can test values of $y \gtrsim 2$. Intriguingly, we noted that if the Standard Model top mass is generated via four-fermion operators, we can naturally explain the wide-width resonance reported by ATLAS.

Our analysis shows that topological sectors from models of dynamical electroweak symmetry breaking leave imprints that can soon be tested by the LHC experiments.

ACKNOWLEDGMENTS

The CP³-Origins center is partially funded by the Danish National Research Foundation, grant number DNR90.

Appendix A: Wess-Zumino-Witten Action

The complete gauge invariant Wess-Zumino-Witten Lagrangian \mathcal{L}_{WZW} , arising from the anomalous divergence of axial-vector currents in the underlying theory, can be expressed in terms of the Maurer-Cartan one-forms

$$\alpha = (\partial_\mu \mathcal{U}) \mathcal{U}^{-1} dx^\mu \equiv (d\mathcal{U}) \mathcal{U}^{-1}, \quad \beta = \mathcal{U}^{-1} \alpha \mathcal{U} \quad (\text{A1})$$

and additional ‘‘left’’ and ‘‘right’’ one-forms, $A_L = A_L^\mu dx_\mu$ and $A_R = A_R^\mu dx_\mu$, respectively, with $A_{L/R}^\mu$ defined in (24). We have

$$\begin{aligned} \int_{M^4} \mathcal{L}_{WZW} = & \Gamma_{WZ}[\mathcal{U}] + 5C \left[i \int_{M^4} \text{Tr} [A_L \alpha^3 + A_R \beta^3] - \int_{M^4} \text{Tr} [(dA_L A_L + A_L dA_L) \alpha + (dA_R A_R + A_R dA_R) \beta] \right. \\ & + \int_{M^4} \text{Tr} [dA_L d\mathcal{U} A_R \mathcal{U}^{-1} - dA_R d\mathcal{U}^{-1} A_L \mathcal{U}] + \int_{M^4} \text{Tr} [A_R \mathcal{U}^{-1} A_L \mathcal{U} \beta^2 - A_L \mathcal{U} A_R \mathcal{U}^{-1} \alpha^2] \\ & + \frac{1}{2} \int_{M^4} \text{Tr} [(A_L \alpha)^2 - (A_R \beta)^2] + i \int_{M^4} \text{Tr} [A_L^3 \alpha + A_R^3 \beta] \\ & + i \int_{M^4} \text{Tr} [(dA_R A_R + A_R dA_R) \mathcal{U}^{-1} A_L \mathcal{U} - (dA_L A_L + A_L dA_L) \mathcal{U} A_R \mathcal{U}^{-1}] \\ & + i \int_{M^4} \text{Tr} [A_L \mathcal{U} A_R \mathcal{U}^{-1} A_L \alpha + A_R \mathcal{U}^{-1} A_L \mathcal{U} A_R \beta] \\ & \left. + \int_{M^4} \text{Tr} \left[A_R^3 \mathcal{U}^{-1} A_L \mathcal{U} - A_L^3 \mathcal{U} A_R \mathcal{U}^{-1} + \frac{1}{2} (\mathcal{U} A_R \mathcal{U}^{-1} A_L)^2 \right] - r \int_{M^4} \text{Tr} [F_L \mathcal{U} F_R \mathcal{U}^{-1}] \right] \quad (\text{A2}) \end{aligned}$$

where $C = -id(R)/(240\pi^2)$ and r is a free parameter which is not determined by the gauge anomaly. Here F_L and F_R are two-forms defined as $F_L = dA_L - iA_L^2$ and $F_R = dA_R - iA_R^2$. The Wess-Zumino effective action is $\Gamma_{WZ}[\mathcal{U}] = C \int_{M^5} \text{Tr}[\alpha^5]$, where M^5 is a five-dimensional manifold whose boundary M^4 denotes the Minkowski space.

-
- [1] G. Aad *et al.* [ATLAS Collaboration], Phys. Lett. B **716**, 1 (2012) [arXiv:1207.7214 [hep-ex]].
- [2] S. Chatrchyan *et al.* [CMS Collaboration], Phys. Lett. B **716**, 30 (2012) [arXiv:1207.7235 [hep-ex]].
- [3] The ATLAS collaboration, ATLAS-CONF-2015-081.
- [4] CMS Collaboration [CMS Collaboration], CMS-PAS-EXO-15-004.
- [5] E. Molinaro, F. Sannino and N. Vignaroli, arXiv:1512.05334 [hep-ph].
- [6] A. Pilaftsis, Phys. Rev. D **93**, no. 1, 015017 (2016) [arXiv:1512.04931 [hep-ph]].
- [7] R. Franceschini *et al.*, arXiv:1512.04933 [hep-ph].
- [8] O. Antipin, M. Mojaza and F. Sannino, arXiv:1512.06708 [hep-ph].
- [9] S. Knapen, T. Melia, M. Papucci and K. Zurek, arXiv:1512.04928 [hep-ph].
- [10] P. S. B. Dev, R. N. Mohapatra and Y. Zhang, arXiv:1512.08507 [hep-ph].
- [11] S. Fichet, G. von Gersdorff and C. Royon, arXiv:1512.05751 [hep-ph].
- [12] C. Csaki, J. Hubisz and J. Terning, Phys. Rev. D **93**, no. 3, 035002 (2016) [arXiv:1512.05776 [hep-ph]].
- [13] C. Csaki, J. Hubisz, S. Lombardo and J. Terning, arXiv:1601.00638 [hep-ph].
- [14] L. A. Harland-Lang, V. A. Khoze and M. G. Ryskin, arXiv:1601.07187 [hep-ph].
- [15] S. I. Godunov, A. N. Rozanov, M. I. Vysotsky and E. V. Zhemchugov, arXiv:1602.02380 [hep-ph].
- [16] A. Djouadi, J. Ellis, R. Godbole and J. Quevillon, arXiv:1601.03696 [hep-ph].
- [17] B. Bellazzini, R. Franceschini, F. Sala and J. Serra, arXiv:1512.05330 [hep-ph].
- [18] D. B. Franzosi and M. T. Frandsen, arXiv:1601.05357 [hep-ph].
- [19] J. Bernon and C. Smith, arXiv:1512.06113 [hep-ph].
- [20] W. S. Cho, D. Kim, K. Kong, S. H. Lim, K. T. Matchev, J. C. Park and M. Park, arXiv:1512.06824 [hep-ph].
- [21] F. P. Huang, C. S. Li, Z. L. Liu and Y. Wang, arXiv:1512.06732 [hep-ph].
- [22] M. Chala, M. Duerr, F. Kahlhoefer and K. Schmidt-Hoberg, Phys. Lett. B **755**, 145 (2016) [arXiv:1512.06833 [hep-ph]].
- [23] L. Aparicio, A. Azatov, E. Hardy and A. Romanino, arXiv:1602.00949 [hep-ph].
- [24] H. An, C. Cheung and Y. Zhang, arXiv:1512.08378 [hep-ph].
- [25] Y. Mambrini, G. Arcadi and A. Djouadi, arXiv:1512.04913 [hep-ph].
- [26] F. D'Eramo, J. de Vries and P. Panci, arXiv:1601.01571 [hep-ph].
- [27] M. Redi, A. Strumia, A. Tesi and E. Vigiani, arXiv:1602.07297 [hep-ph].
- [28] P. Di Vecchia and G. Veneziano, Phys. Lett. B **95**, 247 (1980).
- [29] K. Harigaya and Y. Nomura, arXiv:1602.01092 [hep-ph].
- [30] J. E. Kim, Phys. Lett. B **755**, 190 (2016) [arXiv:1512.08467 [hep-ph]].
- [31] N. D. Barrie, A. Kobakhidze, M. Talia and L. Wu, arXiv:1602.00475 [hep-ph].
- [32] W. Liao and H. q. Zheng, arXiv:1512.06741 [hep-ph].
- [33] J. M. No, V. Sanz and J. Setford, arXiv:1512.05700 [hep-ph].
- [34] K. Harigaya and Y. Nomura, Phys. Lett. B **754**, 151 (2016) [arXiv:1512.04850 [hep-ph]].
- [35] J. M. Cline and Z. Liu, arXiv:1512.06827 [hep-ph].
- [36] A. Belyaev, G. Cacciapaglia, H. Cai, T. Flacke, A. Parolini and H. Serdio, arXiv:1512.07242 [hep-ph].
- [37] E. Witten, Nucl. Phys. B **223**, 433 (1983).
- [38] J. Wess and B. Zumino, Phys. Lett. B **37**, 95 (1971).
- [39] O. Kaymakcalan and J. Schechter, Phys. Rev. D **31**, 1109 (1985).
- [40] O. Kaymakcalan, S. Rajeev and J. Schechter, Phys. Rev. D **30**, 594 (1984).
- [41] J. Schechter, Phys. Rev. D **34**, 868 (1986).
- [42] Z. y. Duan, P. S. Rodrigues da Silva and F. Sannino, Nucl. Phys. B **592**, 371 (2001) [hep-ph/0001303].
- [43] G. Aad *et al.* [ATLAS Collaboration], JHEP **1512**, 055 (2015) [arXiv:1506.00962 [hep-ex]].
- [44] CMS Collaboration [CMS Collaboration], CMS-PAS-EXO-14-010.
- [45] J. Steinberger, Phys. Rev. **76**, 1180 (1949).
- [46] S. Fichet, G. von Gersdorff, O. Kepka, B. Lenzi, C. Royon and M. Saimpert, Phys. Rev. D **89**, 114004 (2014) [arXiv:1312.5153 [hep-ph]].
- [47] S. Fichet, G. von Gersdorff, B. Lenzi, C. Royon and M. Saimpert, JHEP **1502**, 165 (2015) [arXiv:1411.6629 [hep-ph]].
- [48] J. Alwall, M. Herquet, F. Maltoni, O. Mattelaer and T. Stelzer, JHEP **1106**, 128 (2011) [arXiv:1106.0522 [hep-ph]].
- [49] R. D. Ball *et al.* [NNPDF Collaboration], Nucl. Phys. B **877**, 290 (2013) [arXiv:1308.0598 [hep-ph]].
- [50] V. M. Budnev, I. F. Ginzburg, G. V. Meledin and V. G. Serbo, Phys. Rept. **15**, 181 (1975).
- [51] A. D. Martin, R. G. Roberts, W. J. Stirling and R. S. Thorne, Eur. Phys. J. C **39**, 155 (2005) [hep-ph/0411040].
- [52] F. Demartin, F. Maltoni, K. Mawatari, B. Page and M. Zaro, Eur. Phys. J. C **74**, no. 9, 3065 (2014) [arXiv:1407.5089 [hep-ph]].
- [53] J. Alwall *et al.*, JHEP **1407**, 079 (2014) [arXiv:1405.0301 [hep-ph]].

- [54] G. Aad *et al.* [ATLAS Collaboration], Phys. Rev. D **92**, no. 3, 032004 (2015) [arXiv:1504.05511 [hep-ex]].
- [55] V. Khachatryan *et al.* [CMS Collaboration], Phys. Lett. B **750**, 494 (2015) [arXiv:1506.02301 [hep-ex]].
- [56] T. Sjostrand, S. Mrenna and P. Z. Skands, JHEP **0605**, 026 (2006) [hep-ph/0603175].
- [57] J. de Favereau *et al.* [DELPHES 3 Collaboration], JHEP **1402**, 057 (2014) [arXiv:1307.6346 [hep-ex]].
- [58] V. Khachatryan *et al.* [CMS Collaboration], Phys. Rev. D **93**, no. 1, 012001 (2016) [arXiv:1506.03062 [hep-ex]].
- [59] V. Khachatryan *et al.* [CMS Collaboration], Phys. Rev. Lett. **116**, no. 7, 071801 (2016) [arXiv:1512.01224 [hep-ex]].
- [60] G. Aad *et al.* [ATLAS Collaboration], Phys. Lett. B **754**, 302 (2016) [Phys. Lett. B **754**, 302 (2016)] [arXiv:1512.01530 [hep-ex]].
- [61] G. Aad *et al.* [ATLAS Collaboration], Phys. Rev. Lett. **114**, no. 22, 221802 (2015) [arXiv:1504.00357 [hep-ex]].
- [62] V. Khachatryan *et al.* [CMS Collaboration], Phys. Rev. D **91**, no. 5, 052009 (2015) [arXiv:1501.04198 [hep-ex]].
- [63] D. B. Kaplan and H. Georgi, Phys. Lett. B **136**, 183 (1984).
- [64] D. B. Kaplan, H. Georgi and S. Dimopoulos, Phys. Lett. B **136**, 187 (1984).
- [65] E. Witten, Phys. Lett. B **117**, 324 (1982).
- [66] R. Foadi, M. T. Frandsen, T. A. Ryttov and F. Sannino, Phys. Rev. D **76**, 055005 (2007) [arXiv:0706.1696 [hep-ph]].
- [67] S. Chatrchyan *et al.* [CMS Collaboration], JHEP **1307**, 122 (2013) [arXiv:1305.0491 [hep-ex]].
- [68] R. Lewis, C. Pica and F. Sannino, Phys. Rev. D **85**, 014504 (2012) [arXiv:1109.3513 [hep-ph]].
- [69] A. Hietanen, R. Lewis, C. Pica and F. Sannino, JHEP **1407**, 116 (2014) [arXiv:1404.2794 [hep-lat]].
- [70] R. Arthur, V. Drach, M. Hansen, A. Hietanen, C. Pica and F. Sannino, arXiv:1602.06559 [hep-lat].
- [71] S. Nussinov, Phys. Lett. B **165**, 55 (1985).
- [72] S. M. Barr, R. S. Chivukula and E. Farhi, Phys. Lett. B **241**, 387 (1990).
- [73] S. B. Gudnason, C. Kouvaris and F. Sannino, Phys. Rev. D **73**, 115003 (2006) [hep-ph/0603014].
- [74] S. B. Gudnason, C. Kouvaris and F. Sannino, Phys. Rev. D **74**, 095008 (2006) [hep-ph/0608055].
- [75] T. A. Ryttov and F. Sannino, Phys. Rev. D **78**, 115010 (2008) [arXiv:0809.0713 [hep-ph]].
- [76] M. T. Frandsen and F. Sannino, Phys. Rev. D **81**, 097704 (2010) [arXiv:0911.1570 [hep-ph]].
- [77] M. T. Frandsen, S. Sarkar and K. Schmidt-Hoberg, Phys. Rev. D **84**, 051703 (2011) [arXiv:1103.4350 [hep-ph]].
- [78] A. Belyaev, M. T. Frandsen, S. Sarkar and F. Sannino, Phys. Rev. D **83**, 015007 (2011) [arXiv:1007.4839 [hep-ph]].
- [79] Y. Hochberg, E. Kuflik, H. Murayama, T. Volansky and J. G. Wacker, Phys. Rev. Lett. **115**, no. 2, 021301 (2015) [arXiv:1411.3727 [hep-ph]].
- [80] M. Hansen, K. Langble and F. Sannino, Phys. Rev. D **92**, no. 7, 075036 (2015) [arXiv:1507.01590 [hep-ph]].
- [81] D. D. Dietrich, F. Sannino and K. Tuominen, Phys. Rev. D **72**, 055001 (2005) [hep-ph/0505059].
- [82] R. Foadi, M. T. Frandsen and F. Sannino, Phys. Rev. D **87**, no. 9, 095001 (2013) [arXiv:1211.1083 [hep-ph]].
- [83] F. Sannino and K. Tuominen, Phys. Rev. D **71**, 051901 (2005) [hep-ph/0405209].
- [84] D. D. Dietrich and F. Sannino, Phys. Rev. D **75**, 085018 (2007) [hep-ph/0611341].
- [85] G. Bergner, T. A. Ryttov and F. Sannino, JHEP **1512**, 054 (2015) [arXiv:1510.01763 [hep-th]].
- [86] S. Catterall and F. Sannino, Phys. Rev. D **76**, 034504 (2007) [arXiv:0705.1664 [hep-lat]].
- [87] A. Hietanen, J. Rantaharju, K. Rummukainen and K. Tuominen, Nucl. Phys. A **820**, 191C (2009).
- [88] L. Del Debbio, B. Lucini, A. Patella, C. Pica and A. Rago, Phys. Rev. D **82**, 014510 (2010) [arXiv:1004.3206 [hep-lat]].
- [89] T. DeGrand, Y. Shamir and B. Svetitsky, Phys. Rev. D **83**, 074507 (2011) [arXiv:1102.2843 [hep-lat]].
- [90] T. Appelquist, G. T. Fleming, M. F. Lin, E. T. Neil and D. A. Schaich, Phys. Rev. D **84**, 054501 (2011) [arXiv:1106.2148 [hep-lat]].
- [91] T. DeGrand, Y. Shamir and B. Svetitsky, Phys. Rev. D **82**, 054503 (2010) [arXiv:1006.0707 [hep-lat]].
- [92] Z. Fodor, K. Holland, J. Kuti, S. Mondal, D. Negradi and C. H. Wong, JHEP **1509**, 039 (2015) [arXiv:1506.06599 [hep-lat]].
- [93] A. Hasenfratz, Y. Liu and C. Y. H. Huang, arXiv:1507.08260 [hep-lat].
- [94] A. Athenodorou, E. Bennett, G. Bergner and B. Lucini, Phys. Rev. D **91**, no. 11, 114508 (2015) [arXiv:1412.5994 [hep-lat]].
- [95] D. D. Dietrich, F. Sannino and K. Tuominen, Phys. Rev. D **73**, 037701 (2006) [hep-ph/0510217].
- [96] Z. Fodor, K. Holland, J. Kuti, D. Negradi, C. Schroeder and C. H. Wong, Phys. Lett. B **718**, 657 (2012) [arXiv:1209.0391 [hep-lat]].
- [97] Z. Fodor, K. Holland, J. Kuti, S. Mondal, D. Negradi and C. H. Wong, PoS LATTICE **2014**, 244 (2015) [arXiv:1502.00028 [hep-lat]].
- [98] Z. Fodor, K. Holland, J. Kuti, S. Mondal, D. Negradi and C. H. Wong, arXiv:1601.03302 [hep-lat].
- [99] H. S. Fukano and F. Sannino, Phys. Rev. D **82**, 035021 (2010) [arXiv:1005.3340 [hep-ph]].
- [100] T. Appelquist and F. Sannino, Phys. Rev. D **59**, 067702 (1999) [hep-ph/9806409].
- [101] B. Holdom, Phys. Lett. B **143**, 227 (1984).
- [102] E. Witten, Nucl. Phys. B **156**, 269 (1979).
- [103] G. Veneziano, Nucl. Phys. B **159**, 213 (1979).
- [104] F. Sannino and M. Shifman, Phys. Rev. D **69**, 125004 (2004) [hep-th/0309252].
- [105] P. Di Vecchia and F. Sannino, Eur. Phys. J. Plus **129**, 262 (2014) [arXiv:1310.0954 [hep-ph]].
- [106] K. A. Olive *et al.* [Particle Data Group Collaboration], Chin. Phys. C **38**, 090001 (2014).